Inorganic Chemistry

Article

pubs.acs.org/IC

Selective Synthesis and Redox Sequence of a Heterobimetallic Nickel/Copper Complex of the Noninnocent Siamese-Twin Porphyrin

Lina K. Blusch,[†,§] Oliver Mitevski,[†] Vlad Martin-Diaconescu,[‡] Kevin Pröpper,[†,∥] Serena DeBeer,[‡] Sebastian Dechert,[†] and Franc Meyer*[,†]

[†]Institut für Anorganische Chemie, Georg-August Universität, Tammannstrasse 4, D-37077 Göttingen, Germany

[‡]MPI für Chemische Energiekonversion, Stiftstrasse 34−36, D-45470 Mülheim an der Ruhr, Germany

Supporting Information

ABSTRACT: The Siamese-twin porphyrin (**1H$_4$**) is a redox noninnocent pyrazole-expanded porphyrin with two equivalent dibasic {N$_4$} binding sites. It is now shown that its selective monometalation can be achieved to give the nickel(II) complex **1H$_2$Ni** with the second {N$_4$} site devoid of a metal ion. This intermediate is then cleanly converted to **1Ni$_2$** and to the first heterobimetallic Siamese-twin porphyrin **1CuNi**. Structural characterization of **1H$_2$Ni** shows that it has the same helical structure previously seen for **1Cu$_2$**, **1Ni$_2$**, and free base **1H$_6^{2+}$**. Titration experiments suggest that the metal-devoid pocket of **1H$_2$Ni** can accommodate two additional protons, giving [**1H$_4$Ni**]$^{2+}$. Both bimetallic complexes **1Ni$_2$** and **1CuNi** feature rich redox chemistry, similar to the recently reported **1Cu$_2$**, including two chemically reversible oxidations at moderate potentials between −0.3 and +0.5 V (vs Cp_2Fe/Cp_2Fe^+). The locus of these oxidations, in singly oxidized [**1Ni$_2$**]$^+$ and [**1CuNi**]$^+$ as well as twice oxidized [**1CuNi**]$^{2+}$, has been experimentally derived from comparison of the electrochemical properties of the complete series of complexes **1Cu$_2$**, **1Ni$_2$**, and **1CuNi**, and from electron paramagnetic resonance (EPR) spectroscopy and X-ray absorption spectroscopy (XAS) (Ni and Cu K edges). All redox events are largely ligand-based, and in heterobimetallic **1CuNi**, the first oxidation takes place within its Cu-subunit, while the second oxidation then occurs in its Ni-subunit. Adding pyridine to solutions of [**1Ni$_2$**]$^+$ and [**1CuNi**]$^{2+}$ cleanly converts them to metal-oxidized redox isomers with axial EPR spectra typical for Ni^{III} having significant $d_{z^2}^1$ character, reflecting close similarity with nickel complexes of common porphyrins. The possibility of selectively synthesizing heterobimetallic complexes **1MNi** from a symmetric binucleating ligand scaffold, with the unusual situation of three distinct contiguous redox sites (M, Ni, and the porphyrin-like ligand), further expands the Siamese-twin porphyrin's potential to serve as an adjustable platform for multielectron redox processes in chemical catalysis and in electronic applications.

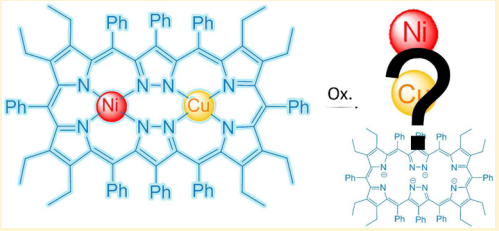

INTRODUCTION

Porphyrins are ubiquitous in nature, and their metal ion complexes have indispensible biological functions such as in chlorophyll and hemoglobin.[1] Because of an allowed $\pi \rightarrow \pi^*$ absorption in the visible region, porphyrins and their complexes are extremely colorful compounds and are thus also referred to as the pigments of life.[2] A plethora of synthetic porphyrin derivatives have been synthesized with variations of the constituent heterocycles, the rings size, and the peripheral substituents. Incorporation of heterocycles other than pyrrole, such as furan, thiole, selenophene, or tellurophene, has generated new platforms for metal complexation.[3] Expansion of the core size by increasing the number of heterocyclic units or the length of the linkages between them has evolved the subfield of expanded porphyrins.[4] These artificial analogues of porphyrins consist of a minimum of 17 atoms within the internal ring.[5] Within their enlarged cavities they can bind lanthanoides,[6] and they can be used to host two metal ions in bimetallic complexes.[7] Hexaphyrin (Chart 1) is a prominent example of an expanded porphyrin and is among the most investigated systems with respect to aromaticity issues.[8] It can adopt various configurations depending on its oxidation state, its substituents, and the orientation of the pyrroles. Most commonly observed are hexaphyrins with two inverted pyrrole units that offer two cavities for binding two proximate metal ions, each with an {N$_2$C$_2$} donor set. While several homo- and heterobimetallic complexes with gold, mercury, and rhodium were synthesized,[7,9] in the case of first row transition metals only monometallic complexes of nickel have been obtained so far.[10] In 2003, Furuta reported on a doubly N-confused hexaphyrin with two {N$_3$C} cavities; subsequent oxygen atom transfer onto the confused pyrrole-CH led to an {N$_3$O} donor set, which finally gave bimetallic nickel and copper complexes using this modified hexaphyrin as a binucleating ligand system.[11] Most recently, Furuta et al. communicated the palladium-induced rearrangement of a singly N-confused to a *cis*-configured doubly N-confused [26]hexaphyrin that contains an {N$_4$} and an {N$_2$C$_2$} cavity.[12]

We recently reported on the synthesis of the first pyrazole-expanded porphyrin which we named the Siamese-twin porphyrin **1H$_4$** (Charts 1 and 2).[13] This system resembles

Received: February 26, 2014
Published: July 11, 2014

   dx.doi.org/10.1021/ic500460n | *Inorg. Chem.* 2014, 53, 7876−7885

Chart 1. Overview of Different [26]Hexaphyrin Constitutions and the Siamese-Twin Porphyrin

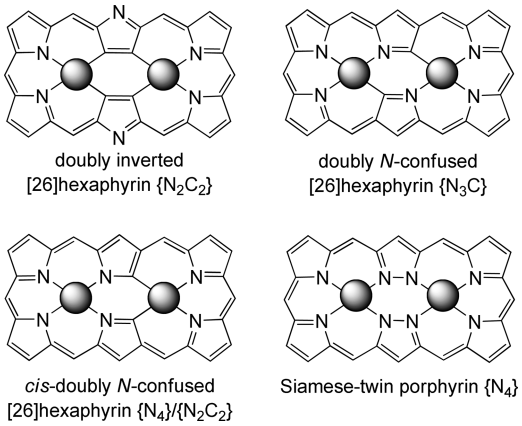

Chart 2. Free-Base Siamese-Twin Porphyrin $1H_4$ Decorated with Substituents at the Periphery

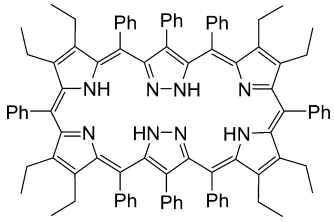

hexaphyrin but with the two inverted pyrrol units substituted by pyrazole, thus offering twice the porphyrin-like $\{N_4\}$ donor set. This architecture appears well suited for forming first row bimetallic complexes, which was already probed by the synthesis of the dicopper(II) and the dinickel(II) complexes.[13,14] In both cases, the metal ions were found in a near square-planar $\{N_4\}$ environment, but X-ray crystallographic analysis as well as spectroscopic studies revealed a highly twisted structure for the free-base ligand as well as the bimetallic complexes. For the latter, the two $\{N_4\}$ coordination planes are almost perpendicular toward each other, which in the case of the dicopper(II) complex leads to orthogonality of the magnetic orbitals and to ferromagnetic coupling ($S = 1$ ground state). The twisted structure is induced by the massive steric crowding in the macrocycle's periphery due to the particular substitution pattern of $\mathbf{1H_4}$ (Chart 2). A detailed investigation of the Siamese-twin porphyrin's dicopper complex in different oxidation states revealed that the first two oxidations are ligand-centered and that the Siamese-twin porphyrin is a multielectron redox active ligand platform with its noninnocence character hidden from X-ray crystallography.[15] Ligand noninnocence is generally observed when metal and ligand based orbital energies are similar,[16] and this phenomenon has attracted significant interest in recent years with bioinorganic relevance and potential applications in catalysis.[17] While numerous investigations concerning the redox chemistry of porphyrins and their complexes have been published,[18] only few studies have addressed the potential noninnocence of expanded porphyrins.[12,19] Obviously, the situation in bimetallic complexes of expanded porphyrins is multifaceted because of the potential presence of both metal−metal and metal−ligand cooperativities.

Here, we present the selective synthesis of a first monometallic complex of the Siamese-twin porphyrin, namely, the monometallic nickel(II) complex $\mathbf{1H_2Ni}$ that has one $\{N_4\}$ pocket vacant. This serves as a valuable intermediate to form, in subsequent reactions, either the dinickel complex $\mathbf{1Ni_2}$ or the first heterobimetallic copper/nickel complex **1CuNi**. Heterobimetallic complexes attract particular interest, e.g., for use in catalysis,[20,21] but the targeted synthesis of heterobimetallic complexes derived from ligands with two identical compartments usually is a challenge since the selective preparation of the monometallic intermediate often marks the bottleneck. In the case of hexaphyrin, this could only be achieved so far using a monometallic gold hexaphyrin complex as intermediate but not yet with two first row transition metal ions.[7c] In their hexaphyrin work, Mori and Osuka applied an excess of $NaAuCl_4$ to obtain the monometalated and dimetalated species simultaneously.[9] We have now found that the insertion of one or two nickel(II) ions into the Siamese-twin porphyrin scaffold can be conveniently controlled by temperature. Compared to its homobimetallic analogues, the heterobimetallic Siamese-twin porphyrin complex **1CuNi** represents an even more intricate situation with respect to its redox properties, namely, with three different potential redox sites: the copper ion, the nickel ion, and the noninnocent ligand framework. In this study, the redox properties of $\mathbf{1Ni_2}$ and **1CuNi** have been addressed by a combination of different spectroscopic methods.

RESULTS AND DISCUSSION

Synthesis of the Homo- and Hetero-Bimetallic Complexes. The direct synthesis of $\mathbf{1Ni_2}$ was previously achieved by heating to reflux for 24 h a solution of $\mathbf{1H_4}$ and $Ni(OAc)_2{\cdot}4\,H_2O$ in CH_2Cl_2/MeOH (1:1). It was now found that stirring a solution of $\mathbf{1H_4}$ with an excess of $Ni(OAc)_2{\cdot}4\,H_2O$ at room temperature yielded the monometallic species $\mathbf{1H_2Ni}$ as the main product (Scheme 1). Traces of the undesired compound $\mathbf{1Ni_2}$ could be separated by column chromatography. In contrast, stirring a solution of $\mathbf{1H_4}$ and $Cu(OAc)_2{\cdot}H_2O$ in the same solvent at room temperature gave the bimetallic complex $\mathbf{1Cu_2}$ directly. Hence, the order of metal ion insertion cannot be reversed, and heterobimetallic **1CuNi** can only be obtained via $\mathbf{1H_2Ni}$ as an intermediate. $\mathbf{1H_2Ni}$ was readily converted with an excess of $Cu(OAc)_2{\cdot}H_2O$ at room temperature to yield **1CuNi**, which was purified via column chromatography. ESI-HRMS measurements for all the complexes matched well with the simulated spectra and showed the parent ion peaks of m/z = 1357.6089 (found 1357.6093) for $[\mathbf{1H_2Ni} + H^+]^+$, 1412.5208 (found 1412.5182) for $[\mathbf{1Ni_2}]^+$, and 1417.5150 (found 1417.5166) for $[\mathbf{1CuNi}]^+$ (Figures S1−S3, Supporting Information). While $\mathbf{1H_2Ni}$ was found to give, under ESI-MS conditions (CH_2Cl_2/MeCN solution), a cationic species $[\mathbf{1H_3Ni}]^+$ by proton capture, the two bimetallic complexes formed cations via oxidation, thus reflecting their propensity to undergo redox processes.

X-ray Crystallography. The molecular structure of $\mathbf{1Ni_2}$ has been communicated previously.[14] Crystals of $\mathbf{1H_2Ni}{\cdot}11$ acetone$\cdot H_2O$ (triclinic space group $P\bar{1}$; see Supporting Information for details) were grown by slow evaporation of a saturated solution of $\mathbf{1H_2Ni}$ in acetone. The molecular structure of $\mathbf{1H_2Ni}$ is shown in Figure 1 (left, and Figure S4, Supporting Information) and reveals the drastic twisting of the Siamese-twin porphyrin scaffold that was also found for free-base $\mathbf{1H_4}$ and for $\mathbf{1Cu_2}$, both in solid state and in solution.[13,14] This twisting has been attributed to steric repulsion between

dx.doi.org/10.1021/ic500460n | Inorg. Chem. 2014, 53, 7876−7885

Scheme 1. Synthesis of the Mono- and Bi-metallic Complexes $1H_2Ni$, $1Ni_2$, and 1CuNi

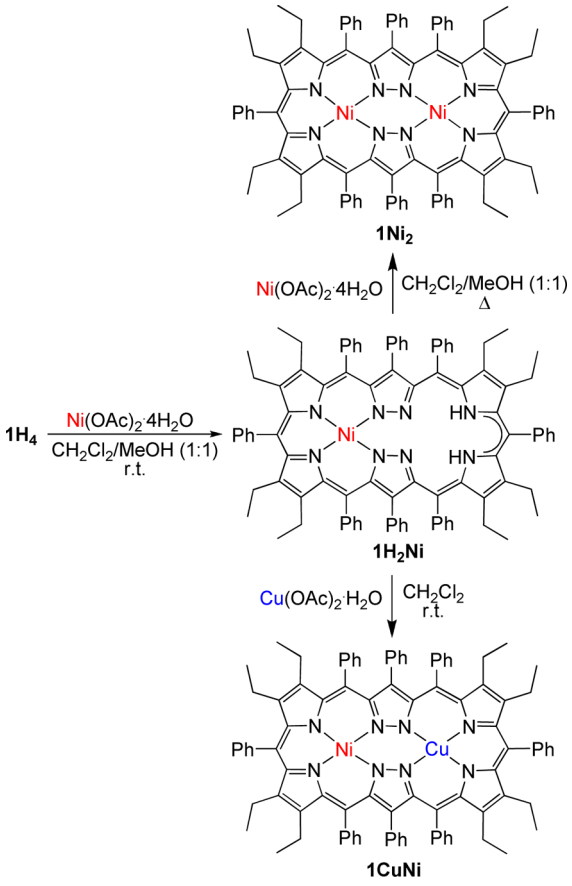

the peripheral substituents. In $1H_2Ni$, one pocket hosts a nickel ion in an almost square planar $\{N_4\}$ coordination environment, while a hydrogen-bound water molecule was found to be located in the metal-free cavity. Defining a mean plane over N1/N2/N3/N4/Ni, the nickel ion is located in plane, and N atoms deviate about ±0.33 Å with N1−Ni−N3 and N2−Ni−N4 angles of ∼160° instead of ideally 180° for a planar square. Although the water molecule located in the metal-free cavity appears to be involved in hydrogen bonding, the azole rings of the metal-devoid subunit are freely oriented with their nitrogen atoms not pointing toward the center of the cavity. Thus, the two pyrazole rings are almost perpendicularly oriented with a dihedral angle N6−N3−N4−N5 of 83°. The overall neutral state of $1H_2Ni$ is confirmed by the absence of any counterions. The molecular structure of $1Ni_2$, obtained from an X-ray diffraction analysis of $1Ni_2$·4 toluene (monoclinic space group $C2/c$) is included in Figure 1 for comparison. Angles N1−Ni−N3 and N2−Ni−N4 are ∼166° in this case.

Both protons in the metal-free cavity of $1H_2Ni$ are found on the pyrrole-N atoms. This unexpected protonation pattern can be explained by electronic effects induced by the nickel(II) ion in the other pocket: binding of the Lewis acidic nickel ion strongly acidifies the pyrazole-NH, resulting in a proton swap. The resulting formally trianionic character of the Ni-containing pocket of $1H_2Ni$ is reflected in N^{pyr}-Ni bonds (1.88 Å) and N^{pz}-Ni bonds (1.87 Å) that are significantly shorter than in $1Ni_2$ (1.90 and 1.92 Å, respectively) with its two formally dianionic porphyrin-like binding sites. The difference is particularly pronounced for the N^{pz}-Ni bonds, indicating the effect of the second nickel(II) ion that is hosted in the adjacent pocket of $1Ni_2$, and the bis(pyrazolato)-bridged bimetallic core.

These findings for $1H_2Ni$ are corroborated by DFT calculations (see Experimental Section and Table S3 (Supporting Information) for details), in which all four possible protonation patterns in the metal-devoid pocket of $1H_2Ni$ were considered, viz. both pyrrole-N protonated, $(HN^{py})_2$; one pyrrole and one pyrazole protonated, $HN^{py}HN^{pz}$; or both pyrazole-N's protonated, $(HN^{pz})_2$. B3LYP single point energies (after geometry optimization using the BP86 functional and including solvent effects using the COSMO model for CH_2Cl_2), suggested that the tautomer $(HN^{py})_2$ with both pyrrole-N's being protonated is indeed most stable, while the $HN^{py}HN^{pz}$ tautomers are slightly higher in energy (by +2.1 and +3.5 kcal/mol), and the $(HN^{pz})_2$ tautomer is significantly disfavored (by +24.2 kcal/mol) (see also Table S3, Supporting Information).

Crystalline material of **1CuNi** was obtained by slow evaporation of a saturated solution of **1CuNi** in toluene; unfortunately, X-ray data obtained from crystals of **1CuNi** could not be fully refined. However, crystalline material was

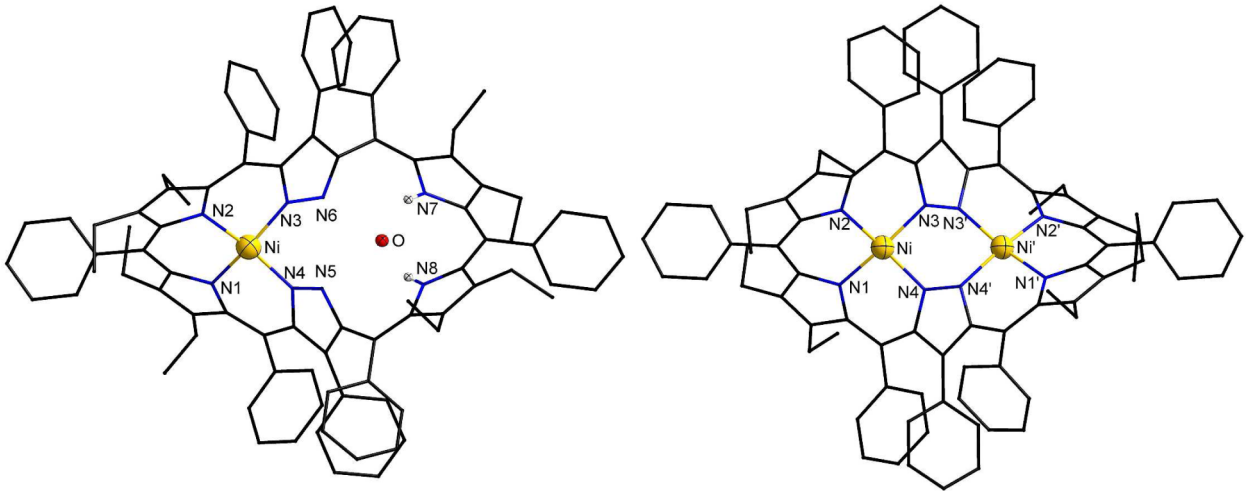

Figure 1. X-ray structures of $1H_2Ni$ (left) and $1Ni_2$ (right)[14] presented in their front views with selected atoms labeled (see also Figure S4, Supporting Information). Selected atom distances are listed in Table S2 in the Supporting Information.

dx.doi.org/10.1021/ic500460n | Inorg. Chem. 2014, 53, 7876−7885

used for all further analyses of the two bimetallic compounds **1Ni$_2$** and **1CuNi**.

Spectroscopic Characterization of 1H$_2$Ni, 1Ni$_2$, and 1CuNi. All three complexes are intensively colored as expected for porphyrinic molecules (Figure 2). While **1H$_2$Ni** is green,

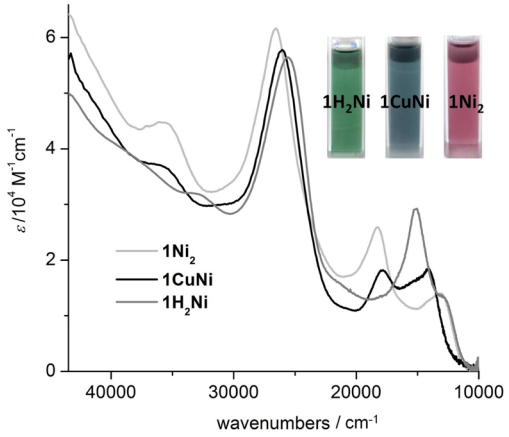

Figure 2. UV−vis spectra of **1H$_2$Ni**, **1Ni$_2$**, and **1CuNi** in CH_2Cl_2.

similar to the color of the free-base ligand itself, complexation of a second nickel ion gives a dark red/purple complex **1Ni$_2$**, whereas **1CuNi** is dark blue. A strong absorption at around 26000 cm^{-1} (~6 × 10^4 $M^{-1}cm^{-1}$) is found for all three complexes, suggesting that this band originates from pure ligand-derived electronic transitions, most likely $\pi \rightarrow \pi^*$ transitions; this is in accordance with MCD spectroscopic results for **1Cu$_2$**.[15] In contrast, the bands between 20000 and 10000 cm^{-1} strongly depend on the number and nature of the bound metal ions.

NMR spectroscopy (Figure 3) confirmed the diamagnetic character of **1H$_2$Ni** and **1Ni$_2$**, which was expected from the roughly square planar coordination geometry (low-spin d^8 nickel(II) electronic configuration). **1H$_2$Ni** with its vacant pocket provides sites for protonation. In its neutral **1H$_2$Ni** form, one NH resonance is found at 14.12 ppm in the ^{1}H NMR spectrum (see Figure S5, Supporting Information). After the addition of two equivalents of trifluoroacetic acid (TFA), the spectral resolution increases and two NH resonances appear at 11.76 and 14.88 ppm (Figures 3 and S5, Supporting Information). These findings indicate a maximum 2-fold protonation giving $[\mathbf{1H_4Ni}]^{2+}$, with both **1H$_2$Ni** and $[\mathbf{1H_4Ni}]^{2+}$ featuring C_2 symmetry along the long axis of the expanded porphyrin molecule.[22] For **1H$_2$Ni**, this is in accordance with the X-ray crystallographic and DFT results which revealed that the two peripheral pyrrole units are protonated, while the pyrazole-N are not (see above). At the level of 1 equiv of TFA addition, differently protonated species coexist (Figure S5, Supporting Information). All downfield signals assigned to NH resonances readily exchange with D_2O.

1Ni$_2$ exhibits D_2 symmetry in solution, which is evidenced by only two distinct ^{1}H NMR triplets for its eight methyl groups and by its ^{13}C NMR spectrum (Figure 3 and Figure S7, Supporting Information). NMR samples for **1Ni$_2$** were prepared from crystalline material and thus show toluene signals. As expected, NH signals at low field have disappeared upon complexation of the second nickel ion.

While the mono- and bimetallic nickel complexes are diamagnetic, **1CuNi** is paramagnetic with a magnetic moment of μ_{eff} = 1.77 μ_B that is almost independent of temperature according to SQUID data (Figure S8, Supporting Information); this is in agreement with an $S = 1/2$ state (spin-only value μ_{eff} = 1.73 μ_B) as expected for the combination of a d^9 copper(II) and a ls-d^8 nickel(II) ion. The low magnetic moment but high molecular weight required that relatively large amounts of material were used for the SQUID measurement, and an accurate diamagnetic correction was applied (using Pascal constants).[23] The almost axial EPR spectrum of **1CuNi** (Figure 4) is typical for tetragonal copper(II) and fairly similar to the

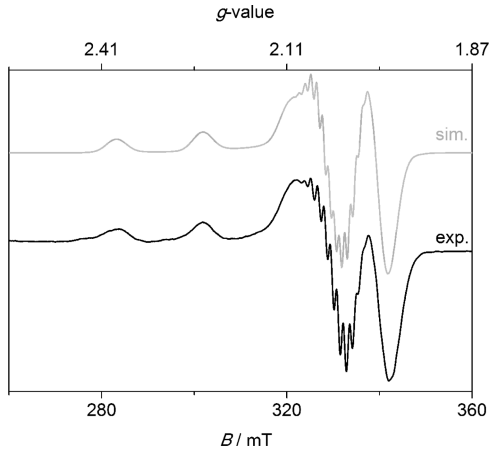

Figure 4. Experimental (black line) and simulated EPR spectrum (gray line) of **1CuNi** at 150 K in CH_2Cl_2 (frozen glass). Data were simulated with g_1 = 2.03, g_2 = 2.06, and g_3 = 2.17, coupling constants of a_{3Cu} = 18.6 mT, a_{1N} = a_{2N} = 1.25 mT, and a_{3N} = 1.00 mT, and line widths of W_1 = 0.6 mT, W_2 = 0.7 mT, and W_3 = 2 mT.

EPR spectrum of nonaggregated copper(II) tetraphenyl porphyrin (Cu(TPP)) and dissymmetric copper(II) porphyrins

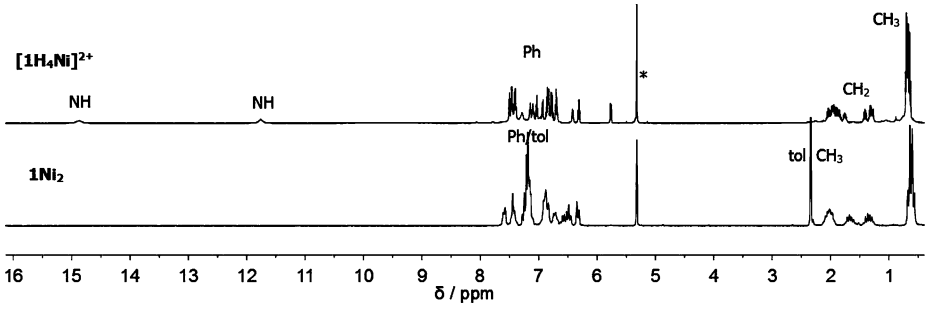

Figure 3. ^{1}H NMR spectra of $[\mathbf{1H_4Ni}]^{2+}$ (500 MHz, CD_2Cl_2, top) and **1Ni$_2$** (200 MHz, CD_2Cl_2, bottom). The asterisk marks the residual solvent signal of CD_2Cl_2; (tol = toluene).

dx.doi.org/10.1021/ic500460n | Inorg. Chem. 2014, 53, 7876−7885

(Table S4, Supporting Information)[24] with splitting into four lines (a_{3Cu} = 18.6 mT) in $g_{\|}$ and hyperfine splitting in the x and y directions into nine lines due to coupling to four ligating N atoms (a_{1N} = a_{2N} = 1.25 mT and a_{3N} = 1.00 mT). The simulation gave g_1 = 2.03, g_2 = 2.06, and g_3 = 2.17, indicating slight rhombicity in accordance with the local symmetry in the Cu subsite of **1CuNi**, which is reduced compared to the 4-fold symmetry of Cu(TPP).

Redox Properties of $1H_2Ni$, $1Ni_2$, and 1CuNi. Complexes of the Siamese-twin porphyrin were designed to serve as multielectron redox reservoirs, potentially involving both the two metal ions and the noninnocent Siamese-twin porphyrin scaffold. Redox properties of $\mathbf{1H_2Ni}$, $\mathbf{1Ni_2}$, and **1CuNi** were first studied using cyclic voltammetry (CV). $\mathbf{1H_2Ni}$ did not show any reversibility in its voltammetric responses (Figure S9, Supporting Information) and thus was not investigated further in this respect. Upon binding a second metal ion, independent of its nature (Ni or Cu), a number of reversible electrochemical processes emerged. In CH_2Cl_2, both bimetallic complexes $\mathbf{1Ni_2}$ and **1CuNi** exhibited five redox waves in the potential window from −2.4 to +1.3 V (versus ferrocene), namely, two reductive and three oxidative processes (Figure 5, Table 1).

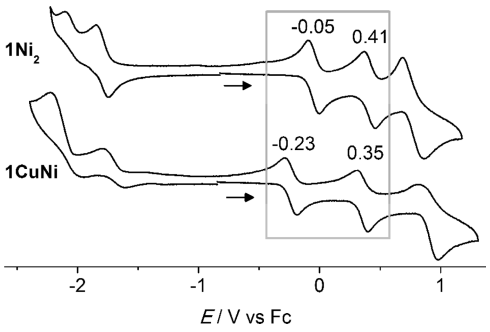

Figure 5. Cyclic voltammograms of $\mathbf{1Ni_2}$ and **1CuNi** in CH_2Cl_2 with $[NBu_4]PF_6$ as the electrolyte and a scan rate of 100 mV; potentials referenced versus the ferrocene (Fc) couple; decamethyl ferrocene was used as internal standard. The gray rectangle marks the chemically reversible conversions that have been studied in more detail.

The CV of $\mathbf{1Ni_2}$ showed three electrochemically reversible processes with half wave potentials at $E_{1/2}$ = −1.79, −0.05, and +0.41 V as well as two electrochemically irreversible or quasi-reversible waves with peak potentials at E_p^{ox} = −2.00/E_p^{red} = −2.10 V and E_p^{ox} = +0.86/E_p^{red} = +0.68 V. **1CuNi** also gave five redox waves but with two electrochemically reversible processes at $E_{1/2}$ = −0.23 and +0.35 V as well as three electrochemically irreversible or quasi-reversible waves at E_p^{ox} = −1.97/E_p^{red} = −2.22 V, E_p^{ox} = −1.61/E_p^{red} = −1.79 V, and E_p^{ox} = +0.98/E_p^{red} = +0.83 V. Each redox step seems to be a one-electron transfer according to square wave voltammetry (SWV), except for the one at lowest potential in the case of $\mathbf{1Ni_2}$ (Figures S12 and S16, Supporting Information). The first two oxidations, shown by the gray rectangle in Figure 5, are electrochemically reversible in both cases and have then been investigated further (see below). Comproportionation constants K_c for the monooxidized products $[\mathbf{1Ni_2}]^+$ and $[\mathbf{1CuNi}]^+$ were calculated from the separation of the half wave potentials[25] as $7.2\cdot10^7$ and $8.1\cdot10^9$, respectively. This indicates significant thermodynamic stability of the monooxidized species.

It should be noted that the related complex $\mathbf{1Cu_2}$ featured two corresponding reversible redox processes at −0.26 V and +0.09 V under identical conditions (CH_2Cl_2, $[NBu_4]PF_6$), giving $[\mathbf{1Cu_2}]^+$ and $[\mathbf{1Cu_2}]^{2+}$ (Table 1).[15] Since the first oxidation of $\mathbf{1Cu_2}$ (at −0.26 V) occurs at almost the same potential as the first oxidation of **1CuNi** (at −0.23 V) while the second oxidation occurs at similar potentials in $\mathbf{1Ni_2}$ and **1CuNi** (at +0.41 and +0.35 V, respectively), it can be assumed that the first oxidation in heterobimetallic **1CuNi** takes place within its Cu-subunit, while the second oxidation is associated with its Ni-subunit (Figure S11, Supporting Information).

Spectroelectrochemistry and Chemical Oxidation. Chemical reversibility of the redox processes was tested on the time scale of bulk electrolysis experiments using UV−vis spectroscopy, which also allowed characterization of the complexes in their various oxidation states. The electrochemical cell was equipped with a UV−vis immersion probe, and the electrochemical processes were followed by UV−vis spectroscopy. Starting with an open circuit potential of about −0.8 V where the neutral species $\mathbf{1Ni_2}$ and **1CuNi** are present, the potentiostat was set to an anodic potential of 0.6 V and subsequently back to −0.8 V (representing the potential range framed by the gray box in Figure 5). After completion of the bulk electrolysis experiment, the initial UV−vis spectra were restored, confirming chemical reversibility of the first two anodic processes (Figure 6 and Figures S12 and S16, Supporting Information). In contrast, the third anodic process as well as the two cathodic processes were shown to be chemically irreversible.

In both cases, $\mathbf{1Ni_2}$ and **1CuNi**, the intensity of the ligand-derived absorption around 26000 cm^{-1} gradually decreased upon sequential oxidation to the mono- and dications, concomitant with a slight shift to lower energies. At the same time, absorptivities in the range from 25000 to around 17000 increased. Changes at even lower energies, in the metal-dependent range from 17000 to 10000, occurred mainly during the first oxidation. Several isosbestic points evidenced direct conversions for both the first and second oxidations.[26] The third oxidation at much higher potential resulted in an overall decrease in spectral intensity but without any isosbestic points. Peak maxima for all species are compiled in the Supporting Information (Tables S5 and S6).

In view of the reversibility of the first two oxidations of $\mathbf{1Ni_2}$ and **1CuNi** and the high stability of the singly oxidized mixed-valence species, the preparation of $[\mathbf{1Ni_2}]^+$ and $[\mathbf{1CuNi}]^+$ was attempted chemically on a preparative scale, using silver(I) salts as the oxidant. Since $[NBu_4]PF_6$ had been used as the electrolyte in the (spectro)electrochemical experiments, $AgPF_6$

Table 1. Electrochemical Parameters for $1Ni_2$, 1CuNi, and $1Cu_2$

	$E_{1/2}$ in V versus the Fc/Fc^+ couple					
$\mathbf{1Ni_2}$	−2.00/−2.10[a]	−1.79	−0.05	0.41	0.86/0.68	
1CuNi	−1.97/−2.22[a]	−1.61/−1.79[a]	−0.23	0.35	0.98/0.83	
$\mathbf{1Cu_2}$[15]	−2.00/−2.14[a]	−1.75	−0.26	0.09	0.99	1.18/1.16[a]

[a]Anodic and cathodic peak potentials E_p^{ox}/E_p^{red}.

dx.doi.org/10.1021/ic500460n | Inorg. Chem. 2014, 53, 7876−7885

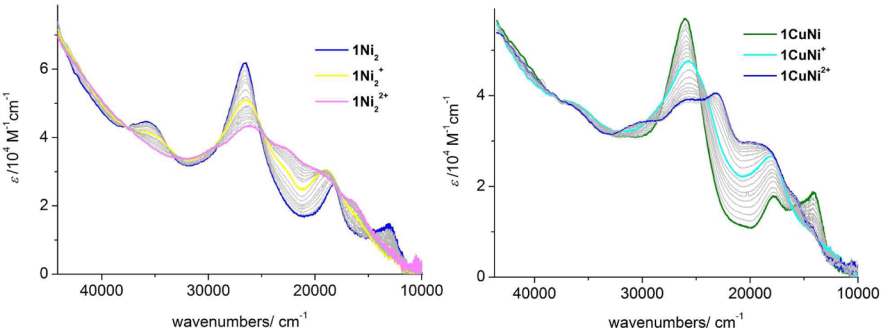

Figure 6. UV−vis spectra of the two first oxidation processes of **1Ni$_2$** and **1CuNi** applying electrochemical conditions (in CH_2Cl_2).

or $AgBF_4$ were deemed the preferred choice in order to ensure similar conditions for both methods, with only weakly coordinating anions present. After the addition of one equivalent of the silver(I) salt (dissolved in nitroethane), UV−vis spectra of the resulting $[\mathbf{1Ni_2}]^+$ and $[\mathbf{1CuNi}]^+$ were very similar to those obtained in the spectroelectrochemical experiments (Figures S13 and S18, Supporting Information). This again confirmed that the individual redox waves in the CVs represent one-electron processes. The monooxidized species (as their BF_4^- or PF_6^- salts) could then be isolated by the removal of all solvents, redissolving the samples in CH_2Cl_2 and filtering off any silver (nano)particles. In this way, the mixed-valence species were available for further analysis without any potentially disturbing excess electrolyte. Unfortunately, however, no crystalline material could be obtained. Samples of the twice oxidized complexes $[\mathbf{1Ni_2}]^{2+}$ and $[\mathbf{1CuNi}]^{2+}$, prepared via chemical oxidation with two equivalents of a silver(I) salt, were prone to decomposition and could not be isolated.

Redox Locus in the Oxidation Products of 1CuNi and 1Ni$_2$. Detailed investigation of the redox sequence of **1Cu$_2$** and of its singly and doubly oxidized species had revealed the noninnocence character of the Siamese-twin porphyrin scaffold with distinct valence localization in the individual subunits.[15] Hence, $[\mathbf{1Cu_2}]^{2+}$ was found to be diamagnetic because of pronounced covalency and strong antiferromagnetic coupling between copper(II) and a ligand-centered radical in each subunit. However, this noninnocence of the Siamese-twin porphyrin was hidden from X-ray crystallography and was poorly described by common DFT methods, the latter systematically favoring delocalization.[15] **1CuNi** with its two different metals now represents an intricate case because of the multitude of possible oxidation sites. Electron paramagnetic resonance (EPR)-, UV−vis-near infrared (NIR)-spectroscopy, and X-ray absorption spectroscopy (XAS) were used to shed light on the oxidation events in this system.

Singly oxidized $[\mathbf{1CuNi}]PF_6$ can be synthesized electrochemically, followed by immediate freezing of the sample solution once transferred into an EPR tube, or chemically. It proved EPR silent in the X-band. The diamagnetic character of $[\mathbf{1CuNi}]^+$ suggests either the presence of Cu^{III} (d^8, $S = 0$) or a ligand centered oxidation within the copper subunit, with strong antiferromagnetic coupling of the Cu^{II} (d^9, $S = 1/2$) to the ligand radical. The latter case would be in line with the locus of redox events found for the dicopper complex and with the diamagnetic character and the electronic structure description of $[\mathbf{1Cu_2}]^{2+}$.[15] However, NMR spectra of $[\mathbf{1CuNi}]PF_6$ were broadened, either due to paramagnetic trace impurities or residual spin density at the ligand. The UV−vis-NIR spectrum of $[\mathbf{1CuNi}]PF_6$ shows a weak broad peak in the NIR region around 5000 cm^{-1}, possibly originating from an IVCT transition between the two ligand halves (ligand-to-ligand IVCT; Figure S20, Supporting Information).

EPR samples of $[\mathbf{1Ni_2}](PF_6)$ were synthesized either electrochemically or chemically as described above. The EPR spectrum of $[\mathbf{1Ni_2}]PF_6$ measured as a frozen solution in CH_2Cl_2 shows a dominant signal of almost axial symmetry $g_\parallel < g_\perp$ with $g_1 = 2.00$, $g_2 = 2.02 \approx g_3 = 2.03$ (sub2; 85%) and a minor subspectrum with $g_1 = 2.10$, $g_2 = 2.34$, and $g_3 = 2.31$ (sub1; 15%) (Figure 7, bottom). Both the g anisotropy ($\Delta g = |g_1 - g_3| = 0.21$) and average g-value ($g_{av} = [(g_1^2 + g_2^2 + g_3^2)/3]^{1/2} = 2.25$) clearly indicate sub1 to correspond to a Ni^{III} species, whereas the major component sub2 originates from a largely ligand-centered radical ($\Delta g = 0.03$, $g_{av} = 2.02$).[27] Similar behavior has also been found for oxidized nickel porphyrin complexes,[28] namely, the coexistence of nickel(III) porphyrin complexes and nickel(II) porphyrinic π-radicals. Furthermore, for oxidized nickel porphyrin complexes conversion to purely metal-oxidized species was observed upon addition of strong axial ligands such as pyridine.[29]

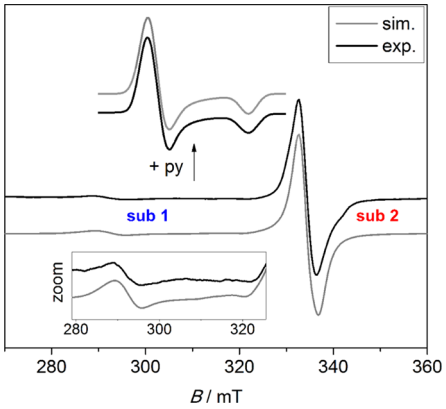

Figure 7. Bottom: X-band EPR spectrum of $[\mathbf{1Ni_2}]PF_6$ at 152 K in CH_2Cl_2 (frozen glass). Data were simulated with $g_1 = 2.10$, $g_2 = 2.34$, and $g_3 = 2.31$ for sub1 and $g_1 = 2.00$, $g_2 = 2.02$, and $g_3 = 2.03$ for sub2. Gaussian line shapes were applied to sub1 (line widths of $W_1 = 4.0$, $W_2 = 8.0$, and $W_3 = 5.0$ mT) and Lorentzian line shapes to sub2 (isotropic line width of 4 mT). The ratio of sub1/sub2 is 15:85. The upper X-band EPR spectrum of $[\mathbf{1Ni_2}]PF_6$ with added excess of pyridine (py) in CH_2Cl_2 at 150 K (frozen glass) was simulated with $g_1 = g_2 = 2.24$ and $g_3 = 2.09$ (line width of $W_1 = 4.1$, $W_2 = 4.4$, and $W_3 = 3.6$ mT with Gaussian line shapes).

In our EPR experiments on $[\mathbf{1Ni_2}]PF_6$, the observation of sub1 may possibly be explained by the presence of potentially

dx.doi.org/10.1021/ic500460n | Inorg. Chem. 2014, 53, 7876−7885

coordinating trace impurities such as chloride ions; indeed, the proportion and appearance of sub1 was variable in multiple experiments, depending on, inter alia, the purity of the solvent used and the duration of storage of the sample (Figure S15, Supporting Information). When pyridine was added, a single purely axial spectrum with $g_1 = g_2 = 2.24$ and $g_3 = 2.09$ was obtained, suggesting that axial coordination of pyridine to the nickel ion (which raises the d_{z^2} orbital in energy) induces full conversion to the metal-oxidized species (Figure 7, top and Scheme 2). Detection of only a single species after the addition

Scheme 2. Simplified Representation of the Proposed Redox Isomerism in the Oxidized Ni-Subunit of $[\mathbf{1Ni_2}]^+$ and $[\mathbf{1CuNi}]^{2+}$ Triggered by Pyridine Coordination[a]

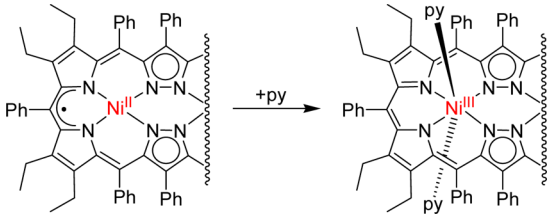

[a]It is not clear though whether one or two pyridines bind to the Ni^{III}.

of pyridine further corroborates that both sub1 and sub2 reflect species derived from the same $[\mathbf{1Ni_2}]^+$ scaffold and that both are transformed to the same pyridine adduct. The relatively low g anisotropy ($\Delta g = 0.15$) and low average g value ($g_{av} = 2.19$) of the pyridine adduct of $[\mathbf{1Ni_2}]PF_6$ suggest significant covalency (i.e., electron delocalization onto the ligand); however, no ^{14}N hyperfine coupling was observed. The UV–vis-NIR spectrum of $[\mathbf{1Ni_2}]PF_6$ did not show any prominent CT band between 10000 and 5000 cm^{-1} (Figure S14, Supporting Information).[30]

The products of the second oxidation of $[\mathbf{1Ni_2}]PF_6$ could not be isolated. EPR spectra of $[\mathbf{1CuNi}](PF_6)_2$, prepared electrochemically or chemically, could be obtained only if the sample solution was frozen immediately. The EPR spectrum of $[\mathbf{1CuNi}](PF_6)_2$ resembles the one of the singly oxidized $[\mathbf{1Ni_2}]PF_6$ complex with the presence of two redox isomers (Figure 8). The isotropy of sub2 ($g_{av} = 2.01$) is characteristic for a ligand-centered radical presenting the dominant species (97%), while the minor axial sub1 spectrum is typical for Ni^{III} with a $d_{z^2}^1$ ground state ($\Delta g = 0.23$; $g_{av} = 2.26$). This suggests that the second oxidation takes place at the ligand subunit where the nickel ion is hosted (and consequently the first oxidation had occurred within the copper-containing subunit), in accordance with the sequence of electrochemical processes (vide supra). After the addition of pyridine, the two subspectra merge into an axial spectrum with $g_1 = g_2 = 2.23$ and $g_3 = 2.11$ ($\Delta g = 0.12$, $g_{av} = 2.19$) (Figure 8, top; Scheme 2); these parameters again suggest a Ni^{III} assignment with significant electron delocalization onto the ligand as has been discussed for $[\mathbf{1Ni_2}]PF_6$.

XAS spectra were measured both at the Cu and Ni K-edges and supported the presence of Cu^{II} and Ni^{II} in singly oxidized $[\mathbf{1CuNi}]PF_6$ and the presence of Ni^{II} in the singly oxidized $[\mathbf{1Ni_2}]PF_6$ (Figure 9). Because of the instability of the doubly oxidized species, XAS data could not be obtained. The Cu K-edge spectra of $[\mathbf{1CuNi}]PF_6$ and $[\mathbf{1Cu_2}](BF_4)_2$[15] are superimposable with overlapping rising edges and 1s to 3d associated pre-edge energies of ~8979.5 eV. This is consistent with the presence of Cu^{II} centers in $[\mathbf{1CuNi}]PF_6$, similar to what was

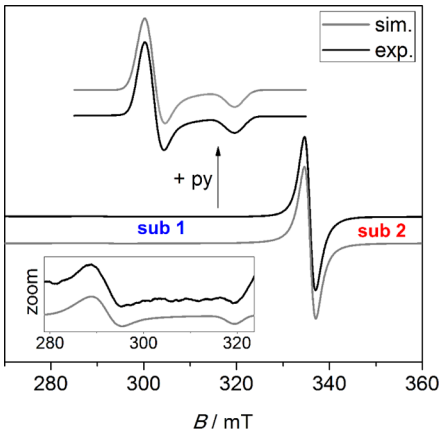

Figure 8. X-band EPR spectrum of $[\mathbf{1CuNi}](PF_6)_2$ at 156 K in CH_2Cl_2 (frozen glass). Data were simulated with $g_1 = 2.34$, $g_2 = 2.31$, and $g_3 = 2.11$ for sub1 and $g_1 = g_2 = 2.01$ and $g_3 = 2.00$ for sub2. Gaussian line shapes were applied to sub1 (line widths of $W_1 = 3.5$, $W_2 = 5.0$, and $W_3 = 8.0$ mT) and Lorentzian line shapes for sub2 (isotropic line width of 4.0 mT). The ratio of sub1/sub2 is around 3:97. The upper X-band EPR spectrum of $[\mathbf{1CuNi}](PF_6)_2$ with added excess of py in CH_2Cl_2 at 140 K (frozen glass) was simulated with $g_1 = g_2 = 2.23$ and $g_3 = 2.11$ (line width of $W = 4$ mT).

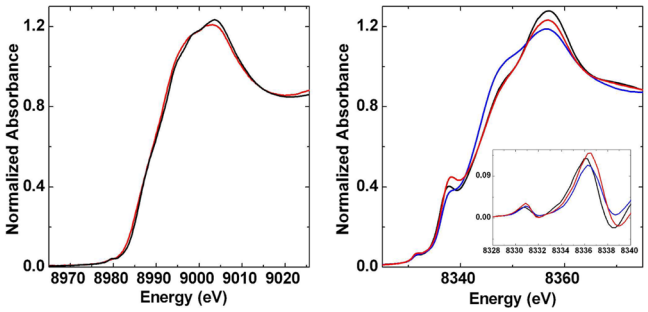

Figure 9. Left: Cu K-edge XAS spectra of $[\mathbf{1CuNi}]PF_6$ (red) and $[\mathbf{1Cu_2}](BF_4)_2$ (black). Right: Ni K-edge XAS spectra of $[\mathbf{1CuNi}]PF_6$ (red), $\mathbf{1Ni_2}$ (black), and $[\mathbf{1Ni_2}]PF_6$ (blue). The inset shows the Ni K-edge 1s to 3d features and 1s to 4p features as a first derivative.

previously reported for $[\mathbf{1Cu_2}](BF_4)_2$.[15,31] The Ni K-edge spectrum of the parent dinickel(II) complex $\mathbf{1Ni_2}$ has a weak pre-edge feature due to 1s to 3d transitions at ~8331.4 eV, followed by a well-resolved feature at ~8337.4 eV corresponding to a 1s to 4p transition. The spectral profile is consistent with a four coordinate square planar Ni^{II} center, such as those reported for Ni-cyclam complexes.[32] The spectrum of $[\mathbf{1CuNi}]PF_6$ has significant similarity with that of $\mathbf{1Ni_2}$. Both the rising edge and the 1s to 3d pre-edge feature (8331.4 eV) of $[\mathbf{1CuNi}]PF_6$ are largely congruent with those of $\mathbf{1Ni_2}$, consistent with a Ni^{II} assignment for $[\mathbf{1CuNi}]PF_6$. Also for $[\mathbf{1Ni_2}]PF_6$, the 1s to 3d pre-edge at 8331.5 eV is similar to that of $\mathbf{1Ni_2}$; however, the rising edge is obscured by higher energy absorption features resulting in a lower apparent energy for the rising edge of $[\mathbf{1Ni_2}]PF_6$ as compared to $\mathbf{1Ni_2}$. Furthermore, the pre-edge intensities of both $[\mathbf{1Ni_2}]PF_6$ and $[\mathbf{1CuNi}]PF_6$ are similar to that of $\mathbf{1Ni_2}$. Within a similar geometric environment, a 2-fold increase is expected in the pre-edge intensity upon oxidation of Ni^{II} to Ni^{III},[32] which clearly is not observed here. Taken together, the data corroborate the presence of Ni^{II} ions in all compounds studied by XAS presented herein. Variations in the 1s to 4p features centered at 8337.5 eV, in the three

dx.doi.org/10.1021/ic500460n | Inorg. Chem. 2014, 53, 7876–7885

compounds, may be attributed to subtle distortions in the coordination geometry and/or differences in covalency (i.e., due to ligand oxidation).[32] These variations should be more pronounced in $[\mathbf{1Ni_2}]PF_6$ than in $[\mathbf{1CuNi}]PF_6$, reflecting that ligand-based oxidation occurs next to one of the Ni^{II} ions in the former, while it likely occurs in the Cu-containing subunit (far from the Ni^{II}) in the latter.

SUMMARY AND CONCLUSIONS

In summary, we synthesized the first heterobimetallic complex of an expanded porphyrin containing only first row transition metals, **1CuNi**. This was achieved via the intermediate monometallic nickel(II) complex $\mathbf{1H_2Ni}$ that has one $\{N_4\}$ pocket of the Siamese-twin porphyrin vacant. According to X-ray crystallography and DFT calculations, the two N-bound protons in the metal-devoid pocket of $\mathbf{1H_2Ni}$ are preferably located at the pyrrole-N, while titration experiments evidence that 2-fold further protonation giving $[\mathbf{1H_4Ni}]^{2+}$ is possible. The isolation and structural characterization of mononuclear $\mathbf{1H_2Ni}$, which can be synthesized with high selectivity despite the symmetry of the pyrazole-expanded porphyrin scaffold, are particularly noteworthy. Preliminary experiments suggest that a variety of other metal ions beyond copper(II) can be subsequently incorporated into the vacant site to give heterobimetallic complexes **1MNi**, which would make $\mathbf{1H_2Ni}$ a very valuable building block in expanded porphyrin chemistry.

Both bimetallic complexes $\mathbf{1Ni_2}$ and **1CuNi** show a rich redox chemistry, similar to that of the recently reported $\mathbf{1Cu_2}$, including two chemically reversible oxidations at moderate potentials between −0.3 and +0.5 V versus the ferrocene couple. The locus of oxidation in the singly oxidized species $[\mathbf{1Ni_2}]^+$ and $[\mathbf{1CuNi}]^+$, as well as in the twice oxidized $[\mathbf{1Ni_2}]^{2+}$ and $[\mathbf{1CuNi}]^{2+}$, was experimentally investigated by a variety of methods. The situation is particularly intricate in **1CuNi** since the copper(II) ion, the nickel(II) ion, and the noninnocent ligand represent three possible oxidation sites. The availability of the complete series of complexes $\mathbf{1Cu_2}$, $\mathbf{1Ni_2}$, and **1CuNi** is beneficial in this respect and allows useful comparisons; the sequence of electrochemical redox events in fact suggested that in heterobimetallic **1CuNi** the first oxidation takes place within its Cu-subunit, while the second oxidation is then associated with its Ni-subunit. Monooxidized complexes $[\mathbf{1Ni_2}]^+$ and $[\mathbf{1CuNi}]^+$ could be synthesized also on a preparative scale using silver(I) salts with noncoordination counterions (BF_4^- and PF_6^-) as oxidants. EPR and XAS revealed that the initial oxidation (and also the second oxidation in case of **1CuNi**) is ligand-centered and that the metal ions stay in the +2 oxidation state throughout. However, trace amounts of Ni^{III} species, recognized from their anisotropic EPR spectra, were often detected for solutions of $[\mathbf{1Ni_2}]^+$ and $[\mathbf{1CuNi}]^{2+}$, and it was found that in the presence of potentially coordinating additives or impurities the electronic structure shifted to the metal-oxidized valence tautomer. Accordingly, the addition of pyridine to solutions of $[\mathbf{1Ni_2}]^+$ and $[\mathbf{1CuNi}]^{2+}$ cleanly converts the EPR spectra to axial ones typical for Ni^{III} with significant $d_{z^2}^1$ electronic character, most likely because of axial pyridine coordination. These effects are reminiscent of what has been frequently observed for nickel complexes of porphyrins and salen-type ligands.

The rich redox chemistry of the Siamese-twin porphyrin's complexes and the multifaceted and adjustable electronic structure of the nickel-containing systems presented in this work, which potentially allows both metal ions together with the noninnocent ligand scaffold to synergistically participate in electron transfer processes, identify this particular expanded porphyrin as a promising platform for use in chemical catalysis and in electronic application.

EXPERIMENTAL SECTION

Materials and Instrumentation. CH_2Cl_2 was purchased from Sigma-Aldrichs in pure analytical grade. Silica gel column chromatography was performed on Machery-Nagel MN60 (0.063−0.2 mm/70−230 mesh ASTM) silica gel. Thin layer chromatography (TLC) was carried out on fluorescence active polyester sheets coated with silica gel Machery-Nagel MN60 (Polygram SIL G/UV_{254}). ^1H and ^{13}C NMR spectra were recorded on Bruker Avance 200, 300, or 500 MHz spectrometers. CV, SWV, and bulk electrolysis were performed using a PerkinElmer 263A potentiostat controlled by electrochemistry power-suit software. CH_2Cl_2 with 0.1 M $[NBu_4]PF_6$ was used as solvent. A glassy carbon electrode was used as a working electrode (a platinum net in case of bulk electrolysis), platinum wire as a counter electrode, and silver wire as a reference electrode. $Cp^*_2Fe/Cp^*_2Fe^+$ was used as internal standard, and potentials were then converted to the Cp_2Fe/Cp_2Fe^+ reference couple.[33] X-band EPR derivative spectra in the temperature range of 120−298 K were recorded on a Bruker ELEXSYS E500 spectrometer, equipped with a ER 049 X microwave bridge, an ER 083 CS magnet, and a digital temperature control system ER 4131 VT using liquid nitrogen as coolant. The microwave frequency of 9.4 GHz was modulated with 5−9 G field modulation amplitude, 100 kHz field modulation frequency, and around 10 mW microwave power. EPR spectra were simulated with the ESIM program developed by E. Bill (Max-Planck Institute for Chemical Energy Conversion, Mülheim/Ruhr, Germany; http://www.cec.mpg.de/menschen/gruppenleiter/molkulare-theorie-und-spektroskopie/eckhard-bill/vita.html) or WinEPR SimFonia.[34] UV−vis spectra were recorded at room temperature with a Varian Cary 50 spectrometer equipped with a glass fiber-optics-cable and a Hellma quartz immersion probe. UV−vis-NIR spectra were recorded on a Varian Cary 5000 spectrophotometer. Susceptibility measurements were carried out with a Quantum-Design MPMS-5S SQUID magnetometer equipped with a 5 T magnet. The powdered sample was contained in a Teflon bucket and fixed in a nonmagnetic sample holder. Each raw data file for the measured magnetic moment was corrected for the diamagnetic contribution of the sample holder and the Teflon bucket. The molar susceptibility data were corrected for the diamagnetic contribution applying Pascals constants. Simulation of the experimental data with full-matrix diagonalization of exchange coupling and Zeeman splitting was performed with the julX program (E. Bill: Max-Planck Institute for Chemical Energy Conversion, Mülheim/Ruhr, Germany; http://www.cec.mpg.de/forschung/molkulare-theorie-und-spektroskopie-molecular-theory-and-spectroscopy/moessbauer-mcd.html). X-ray absorption spectroscopy on solid samples diluted with boron nitride was run at SSRL (Stanford Synchrotron Radiation Lightsource, 3 GeV ring) beamline 7−3 equipped with a Si(220) phi = 90° double crystal monochromator. Data were collected in transmission mode, under a helium cryostat at 10 K. Data averaging and energy calibration were performed using SixPack.[35] The first inflection points from the XANES spectral regions were set to 8980.3 eV for Cu foil (Cu samples) and to 8331.6 eV for Ni foil (Ni samples). The AUTOBK algorithm available in the Athena software package was employed for data reduction and normalization.[36]

Monometallic Nickel(II) Complex $\mathbf{1H_2Ni}$. The mononuclear complex $\mathbf{1H_2Ni}$ was synthesized by adding $Ni(OAc)_2{\cdot}4\,H_2O$ (114 mg, 0.46 mM, 6 equiv) to a solution of $\mathbf{1H_4}$ (100 mg, 0.08 mmol) in CH_2Cl_2 (10 mL) and MeOH (10 mL). The mixture was stirred for 15 min at r.t., and the reaction was monitored via TLC. After removing the solvent under reduced pressure, the purification was done using column chromatography (*n*-hexane/EtOAc 4:1). The obtained dark green product $\mathbf{1H_2Ni}$ was recrystallized from acetone to yield 87 mg (83%). Because of better spectral resolution, NMR data were collected (and detailed assignment has been made) for twice protonated $[\mathbf{1H_4Ni}]^{2+}$ synthesized by addition of 2 equiv of TFA or acetic acid to

dx.doi.org/10.1021/ic500460n | Inorg. Chem. 2014, 53, 7876−7885

$1H_2Ni$: ^{1}H NMR (500 MHz, CD_2Cl_2) δ 0.63−0.73 (m, 24H, CH_3), 1.25−1.46 (m, 6H, CH_2), 1.70−2.09 (m, 12H, CH_2), 5.76 (d, J = 7.6 Hz, 2H, Ph), 6.31 (t, J = 7.5 Hz, 2H, Ph), 6.42 (d, J = 7.4 Hz, 2H, Ph), 6.64−6.90 (m, 12H, Ph), 6.93 (d, J = 7.6 Hz, 2H, Ph), 7.03 (t, J = 7.4 Hz, 2H, Ph), 7.10 (t, J = 7.5 Hz, 2H, Ph), 7.15 (d, J = 7.6, 2H, Ph), 7.24−7.55 (m, 14H, Ph), 11.76 (s, NH), 14.88 (s, NH) ppm; signals for NH at 11.76 and 14.88 integrate to less than the expected 2H each, likely because of severe signal broadening. ^{13}C NMR (125 MHz, CD_2Cl_2): δ 14.7 (CH_3), 14.8 (CH_3), 15.9 (CH_3), 16.3 (CH_3), 19.1 (CH_2), 19.4 ($2CH_2$), 20.3 (CH_2), 105.6, 111.0, 120.4, 122.1, 124.0, 126.0, 126.3 (Ph), 127.0 (Ph), 127.2 (Ph), 127.3, 127.6 (Ph), 128.3 (Ph), 128.4 (Ph), 128.5 (Ph), 128.6 (Ph), 129.0 (Ph), 129.1 (Ph), 129.4, 130.9, 131.7 (Ph), 131.8 (Ph), 131.9, 132.5, 132.7 (Ph), 134.0 (Ph), 134.2 (Ph), 135.4, 137.5, 138.0, 138.6, 145.2, 145.4, 146.7, 147.1, 147.4, 147.9, 149.9, 151.5, 159.9, 160.4 ppm. MS (ESI$^+$, CH_2Cl_2/MeCN): m/z (%): 1357.4 (100) $[M]^+$, 679.5 (54) $[M^{2+}]$. HRMS (ESI$^+$, CH_2Cl_2/MeCN): m/z (%): 1357.6093 (calcd 1357.6089) $[M]^+$. IR (KBr): ν;$^{\sim}$/cm^{-1}: 2970 (w), 1635 (m), 1507 (s), 1437 (m), 1113 (w), 1056 (w), 1016 (w), 697 (m). UV−vis/cm^{-1} (ε/10^4 M^{-1}cm^{-1}): 12853 (1.3), 15128 (2.9), 25381 (5.6), 33003 (3.2).

Heterobimetallic Copper(II) Nickel(II) Complex 1CuNi. Cu(OAc)$_2$·4 H_2O (14.7 mg, 0.07 mM, 1 equiv) was added to **$1H_2Ni$** (100 mg, 0.07 mM) in CH_2Cl_2 (10 mL), and the reaction mixture was stirred for 10 min. The reaction was monitored via TLC. The solvent was removed under reduced pressure, and the crude product was then purified via column chromatography (*n*-hexane/EtOAc 2:1) to yield **1CuNi** (90.1 mg, 87%). Crystalline material was obtained via slow evaporation of a saturated solution of **1CuNi** in toluene. MS (ESI$^+$, CH_2Cl_2/MeCN): m/z (%) 1419.3 (100) $[M]^+$. HRMS (ESI$^+$, CH_2Cl_2/MeCN): m/z (%) 1417.5166 (calcd 1417.5150) $[M]^+$. IR (KBr) ν;$^{\sim}$/cm^{-1}: 2963 (m), 1635 (w), 1457 (m), 1261 (m), 1100 (vs), 1018 (vs), 801 (s), 694 (m). UV−vis/cm^{-1} (ε/10^4 M^{-1}cm^{-1}): 35842 (3.6), 25974 (5.7), 17889 (1.8), 14085 (1.8). Anal. Calcd for $C_{92}H_{80}N_8CuNi$·4 toluene·2 H_2O: C 79.00; H 6.41; N 6.14; Cu 3.48; Ni 3.22. Found: C 78.76; H 6.23; N 6.44; Cu 3.35; Ni 2.23. EPR (150 K, CH_2Cl_2): g_1 = 2.03, g_2 = 2.06, and g_3 = 2.17, a_{3Cu} = 18.6 mT, a_{xN} = a_{yN} = 1.25 mT, a_{zN} = 1.00 mT (line width W_1 = 0.6 mT, W_2 = 0.7 mT, and W_3 = 2 mT).

Homobimetallic Dinickel(II) Complex $1Ni_2$. Ni(OAc)$_2$·4 H_2O (382 mg, 1.54 mmol, 20 equiv) was added to a solution of the Siamese-twin porphyrin **$1H_4$** (0.10 g, 77.0 μmol) in a mixture of CH_2Cl_2 (5 mL) and MeOH (10 mL). The reaction mixture was heated to reflux for 24 h, and the reaction was monitored via TLC. The solvent was removed under reduced pressure and the crude solid product purified by column chromatography (silica, *n*-hexane/EtOAc 4:1). The red-purple fraction was isolated and evaporated to dryness. Crystalline material was obtained via slow evaporation of a saturated solution of **$1Ni_2$** dissolved in toluene. ^{1}H NMR (200 MHz, CD_2Cl_2): δ 0.60 (t, 12H, CH_3), 0.64 (t, 12H, CH_3), 1.29−1.43 (m, 4H, CH_2), 1.58−1.73 (m, 4H, CH_2), 1.92−2.10 (m, 8H, CH_2), 6.28−7.64 (m, 40H, Ph) ppm. ^{13}C NMR (125 MHz, CD_2Cl_2): δ 15.4, 16.0, 19.1, 19.6, 125.2, 126.6, 126.9, 127.4, 127.5, 128.0, 128.2, 146.3, 148.7 ppm. MS (ESI$^+$, CH_2Cl_2/MeCN): m/z (%) 1413.5 (100) $[M]^+$. HRMS (ESI$^+$, CH_2Cl_2/MeCN): m/z (%) 1412.5187 (calcd 1412.5208) $[M]^+$. IR (KBr) ν;$^{\sim}$/cm^{-1}: 2963 (w), 1635 (w), 1457 (m), 1261 (m), 1110 (vs), 1018 (vs), 801 (s), 694 (m). UV−vis/cm^{-1} (ε /10^4 M^{-1}cm^{-1}): 13055 (1.4), 18282 (2.6), 26596 (6.1). Anal. Calcd for $C_{92}H_{80}Ni_2N_8$·4 toluene: C 80.81; H 6.33; N 6.28. Found: C 80.54; H 6.08; N 6.32.

One-Electron Oxidized Dinickel Complex $[1Ni_2]^+$. To a solution of **$1Ni_2$**·4 toluene (10.0 mg, 5.6 μmol) in CH_2Cl_2 (10 mL, pur analytical grade) was added 56.1 μL of a 0.1 M stock solution of $AgPF_6$ or $AgBF_4$ (1 equiv) in nitroethane, and the reaction mixture was stirred for a few seconds. Reaction control was performed using UV−vis spectroscopy. The sample was evaporated to dryness, then taken up in pure CH_2Cl_2 and filtered. The solvent of the filtrate was removed using rotary evaporation. The red product (yield 7.6 mg of $[1Ni_2]BF_4$) was used. The red product was used as obtained and stored under inert conditions. UV−vis/cm^{-1} (ε/10^4 M^{-1} cm^{-1}): 35587 (4.1), 26525 (5.9), 22883 (3.4), 19084 (3.0). EPR (156 K, CH_2Cl_2): sub1 g_1 = 2.10, g_2 = 2.34, and g_3 = 2.31 (line width W_1 = 4.0, W_2 = 8.0, and W_3 = 5.0 mT; Gaussian line shape); sub2 g_1 = 2.00, g_2 = 2.02, and g_3 = 2.03 (isotropic line width of 4 mT; Lorentzian line shapes). The ratio of sub1/sub2 is 15:85.

Twice Oxidized Dinickel Complex $[1Ni_2](PF_6)_2$. Parent **$1Ni_2$** (10 mg, 5.6 μmol) was dissolved in CH_2Cl_2 (10 mL), and 112.2 μL of a 0.1 M stock solution of $AgPF_6$ (or $AgBF_4$) (2 equiv) in nitroethane was added. The reaction mixture was stirred for a few seconds. Isolation of solid $[1Ni_2](PF_6)_2$ (or $[1Ni_2](BF_4)_2$) was not achievable due to decomposition. UV−vis/cm^{-1} (ε/10^4 M^{-1} cm^{-1}): 27322 (3.7), 26110 (4.4), 22883 (3.8), 19763 (3.1), 16474 (2.2).

One-Electron Oxidized Copper Nickel Complex $[1CuNi]^+$. To a solution of **1CuNi**·4 toluene (10 mg, 5.6 μmol) in CH_2Cl_2 (10 mL) was added 56.1 μL of a 0.1 M stock solution of $AgPF_6$ or $AgBF_4$ (1 equiv) in nitroethane, and the reaction mixture was stirred for a few seconds. Reaction control, purification, and storage were handled as with $[1Ni_2]^+$. UV−vis/cm^{-1} (ε/10^4 M^{-1}cm^{-1}): 36900 (3.9), 25707 (4.8), 17986 (2.7), 14599 (1.1).

Twice Oxidized Copper Nickel Complex $[1CuNi](PF_6)_2$. To a solution of **1CuNi** (28 mg, 20 μmol) in CH_2Cl_2 (15 mL), 400 μL of a 0.1 M stock solution of $AgPF_6$ (or $AgBF_4$) (2 equiv) in nitroethane was added. The reaction mixture was stirred for a few seconds. Reaction control, purification, and storage were handled as with $[1Ni_2]^+$. UV−vis/cm^{-1} (ε/10^4 M^{-1} cm^{-1}): 36900 (3.8), 30211 (3.4), 26247 (3.8), 23148 (4.0), 19011 (2.9), 15823 (1.8). EPR (156 K, CH_2Cl_2): g_1 = 2.34, g_2 = 2.31, and g_3 = 2.11 (line widths W_1 = 3.5, W_2 = 5.0, and W_3 = 8.0 mT, Gaussian line shapes) sub2 g_1 = g_2 = 2.01, g_3 = 2.00 (isotropic line width of 4.0 mT, Lorentzian line shapes). The ratio of sub1/sub2 is 3:97.

DFT Calculations. Computations were performed using the ORCA software package 3.0.1.[37] Geometry optimizations were run with the BP86 functional[38] considering solvent effects using the cosmo solvation model (CH_2Cl_2). The def2-sv(p)[39] basis set was employed for C and H atoms, whereas def2-tzvp[39b,40] was employed for Ni and N atoms. Initial coordinates were taken from the experimental crystal structure, and the protonation pattern was modified for the four calculations. Single point energies on these were performed using the B3LYP[38a,41] functional and the def2-tzvp basis set considering solvent effects (cosmo solvation model with CH_2Cl_2).

■ ASSOCIATED CONTENT

Ⓢ Supporting Information

Crystallographic data and plot of the molecular structure of **1H2Ni**·11acetone·H_{2O} with anisotropic displacement ellipsoids and tables with bond lengths and angles; additional spectroscopic, electrochemical and magnetic data; details on DFT calculations. This material is available free of charge via the Internet at http://pubs.acs.org. We thank Dr. A. C. Stückl (Göttingen) for some EPR measurements.

■ AUTHOR INFORMATION

Corresponding Author

*E-mail: franc.meyer@chemie.uni-goettingen.de.

Present Address

[§](L.K.B.) University of British Columbia, Vancouver, BC.

Notes

The authors declare no competing financial interest.

[∥]K.P. passed away during the revision of this manuscript.

■ ACKNOWLEDGMENTS

Support by the Fonds der Chemischen Industrie (Ph.D. scholarship to L.K.B.) is gratefully acknowledged. Portions of the research were carried out at the Stanford Synchrotron Radiation Lightsource (SSRL), a national user facility operated by Stanford University on behalf of the DOE, BES. The SSRL SMB Program is supported by DOE, BER, and NIH, NCRR, and BMTP.

REFERENCES

(1) (a) Dolphin, D. *The Porphyrins*. Academic Press: New York, 1978. (b) Messerschmidt, A.; Huber, R.; Poulos, K.; Wieghardt, K. *Handbook of Metalloproteins*; John Wiley & Sons Inc.: Chichester, U.K., 2001.

(2) Battersby, A. R. *Nat. Prod. Rep.* **2000**, *17*, 507−526.

(3) (a) Arnold, L.; Muellen, K. *J. Porphyrins Phthalocyanines* **2011**, *15*, 757−779. (b) Yedukondalu, M.; Ravikanth, M. *Coord. Chem. Rev.* **2011**, *255*, 547−573.

(4) Saito, S.; Osuka, A. *Angew. Chem., Int. Ed.* **2011**, *50*, 4342−4373.

(5) Sessler, J. L.; Gebaur, A.; Weghorn, S. J. Heteroporphyrins, Expanded Porphyrins and Related Macrocycles. In *The Porphyrin Handbook*; Kadish, K. M., Smith, K. M., Guilard, R., Eds.; Academic Press: San Diego, CA, 2000; Vol. *2*, pp 1−413.

(6) (a) Burrell, A. K.; Cyr, M. J.; Lynch, V.; Sessler, J. L. *J. Chem. Soc., Chem. Commun.* **1991**, 1710−1713. (b) Sessler, J. L.; Vivian, A. E.; Seidel, D.; Burrell, A. K.; Hoehner, M.; Mody, T. D.; Gebauer, A.; Weghorn, S. J.; Lynch, V. *Coord. Chem. Rev.* **2001**, *216*−*217*, 411−434.

(7) (a) Mori, A.; Shimizu, S.; Shin, J.-Y.; Osuka, A. *Inorg. Chem.* **2007**, *46*, 4374−4376. (b) Mori, S.; Kim, K. S.; Yoon, Z. S.; Noh, S. B.; Kim, D.; Osuka, A. *J. Am. Chem. Soc.* **2007**, *129*, 11344−11345. (c) Mori, S.; Osuka, A. *Inorg. Chem.* **2008**, *47*, 3937−3939.

(8) (a) Suzuki, M.; Osuka, A. *Chem. Commun.* **2005**, 3685−3687. (b) Koide, T.; Youfu, K.; Saito, S.; Osuka, A. *Chem. Commun.* **2009**, 6047−6049.

(9) Mori, S.; Osuka, A. *J. Am. Chem. Soc.* **2005**, *127*, 8030−8031.

(10) Mori, S.; Shimizu, S.; Taniguchi, R.; Osuka, A. *Inorg. Chem.* **2005**, *44*, 4127−4129.

(11) (a) Srinivasan, A.; Ishizuka, T.; Osuka, A.; Furuta, H. *J. Am. Chem. Soc.* **2003**, *125*, 878−879. (b) Suzuki, M.; Yoon, M.-C.; Kim, D. Y.; Kwon, J. H.; Furuta, H.; Kim, D.; Osuka, A. *Chem.−Eur. J.* **2006**, *12*, 1754−1759.

(12) Gokulnath, S.; Nishimura, K.; Toganoh, M.; Mori, S.; Furuta, H. *Angew. Chem., Int. Ed.* **2013**, *52*, 6940−6943.

(13) Frensch, L. K.; Pröpper, K.; John, M.; Demeshko, S.; Brückner, C.; Meyer, F. *Angew. Chem., Int. Ed.* **2011**, *50*, 1420−1424.

(14) Blusch, L. K.; Hemberger, Y.; Pröpper, K.; Dittrich, B.; Witterauf, F.; John, M.; Bringmann, G.; Brückner, C.; Meyer, F. *Chem.−Eur. J.* **2013**, *19*, 5868−5880.

(15) Blusch, L. K.; Craigo, K. E.; Martin-Diaconescu, V.; McQuarters, A. B.; Bill, E.; Dechert, S.; DeBeer, S.; Lehnert, N.; Meyer, F. *J. Am. Chem. Soc.* **2013**, *135*, 13892−13899.

(16) (a) Ward, M. D.; McCleverty, J. A. *J. Chem. Soc., Dalton Trans.* **2002**, *0*, 275−288. (b) Eisenberg, R. *Coord. Chem. Rev.* **2011**, *255*, 825−836. (c) Schauer, P. A.; Low, P. J. *Eur. J. Inorg. Chem.* **2012**, *2012*, 390−411.

(17) (a) Chirik, P. J.; Wieghardt, K. *Science* **2010**, *327*, 794−795. (b) Dzik, W. I.; de Bruin, B. Open-Shell Organometallics: Reactivity at the Ligand. In *Organometallic Chemistry*; The Royal Society of Chemistry: Cambridge, U.K., 2011; Vol. *37*, pp 46−78. (c) Praneeth, V. K. K.; Ringenberg, M. R.; Ward, T. R. *Angew. Chem., Int. Ed.* **2012**, *51*, 10228−10234. (d) Kaim, W. *Eur. J. Inorg. Chem.* **2012**, *2012*, 343−348.

(18) Kadish, K. M.; Caemelbecke, E. V.; Royal, G. *Electrochemistry of Metallo-Porphyrins in Nonaqueous Media*; Academic Press: San Diego, CA, 2000; Vol. *8*.

(19) (a) Mayer, I.; Nakamura, K.; Srinivasan, A.; Furuta, H.; Toma, H. E.; Araki, K. *J. Porphyrins Phthalocyanines* **2005**, *09*, 813−820. (b) Gokulnath, S.; Yamaguchi, K.; Toganoh, M.; Mori, S.; Uno, H.; Furuta, H. *Angew. Chem., Int. Ed.* **2011**, *50*, 2302−2306.

(20) Stephan, D. W. *Coord. Chem. Rev.* **1989**, *95*, 41−107.

(21) Cooper, B. G.; Napoline, J. W.; Thomas, C. M. *Catal. Rev.: Sci. Eng.* **2012**, 1−40.

(22) It cannot be safely excluded that integration of these ^{1}H NMR resonances is inaccurate because of their broadness. Each signal should represent two chemically equivalent NH signals.

(23) (a) O'Connor, C. J. *Prog. Inorg. Chem.* **1982**, *29*, 203−283. (b) Kahn, O. *Molecular Magnetism*; Wiley-VCH: Weinheim, Germany, 1993. (c) Bain, G. A.; Berry, J. F. *J. Chem. Educ.* **2008**, *85*, 532.

(24) (a) Heinze, K.; Reinhart, A. *Dalton Trans.* **2008**, 469−480. (b) Wolberg, A.; Manassen, J. *J. Am. Chem. Soc.* **1970**, *92*, 2982−2991.

(25) (a) Heinze, J. *Angew. Chem., Int. Ed.* **1984**, *23*, 831−847. (b) Kaim, W.; Klein, A.; Glöckle, M. *Acc. Chem. Res.* **2000**, *33*, 755−763.

(26) Drago, R. S. *Physical Methods for Chemists*, 2nd ed.; Saunders College Publishing: Philadelphia, PA, 1992.

(27) (a) Emeleus, H. J. *Advances in Inorganic Chemistry and Radiochemistry*; Academic Press: New York, 1970; Vol. *13*. (b) Storr, T.; Wasinger, E. C.; Pratt, R. C.; Stack, T. D. P. *Angew. Chem., Int. Ed.* **2007**, *46*, 5198−5201.

(28) Renner, M. W.; Fajer, J. *J. Biol. Inorg. Chem.* **2001**, *6*, 823−830.

(29) (a) Dolphin, D.; Niem, T.; Felton, R. H.; Fujita, I. *J. Am. Chem. Soc.* **1975**, *97*, 5288−5290. (b) Chang, D.; Malinski, T.; Ulman, A.; Kadish, K. M. *Inorg. Chem.* **1984**, *23*, 817−824. (c) Kim, D.; Miller, L. A.; Spiro, T. G. *Inorg. Chem.* **1986**, *25*, 2468−2470. (d) Connick, P. A.; Macor, K. A. *Inorg. Chem.* **1991**, *30*, 4654−4663. (e) Seth, J.; Palaniappan, V.; Bocian, D. F. *Inorg. Chem.* **1995**, *34*, 2201−2206.

(30) (a) Allen, G. C.; Hush, N. S. *Prog. Inorg. Chem.* **1967**, *8*, 357−390. (b) Day, P.; Hush, N. S.; Clark, R. J. H. *Philos. Trans. R. Soc. A* **2008**, *366*, 5−14. (c) D'Alessandro, D. M.; Keene, F. R. *Chem. Soc. Rev.* **2006**, *35*, 424−440.

(31) Sarangi, R.; Aboelella, N.; Fujisawa, K.; Tolman, W. B.; Hedman, B.; Hodgson, K. O.; Solomon, E. I. *J. Am. Chem. Soc.* **2006**, *128*, 8286−8296.

(32) Colpas, G. J.; Maroney, M. J.; Bagyinka, C.; Kumar, M.; Willis, W. S.; Suib, S. L.; Mascharak, P. K.; Baidya, N. *Inorg. Chem.* **1991**, *30*, 920−928.

(33) Connelly, N. G.; Geiger, W. E. *Chem. Rev.* **1996**, *96*, 877−910.

(34) *WinEPR SimFonia*, version 1.25; Bruker Analytische Messtechnik GmbH: Rheinstetten, 1996.

(35) Webb, S. M. *Phys. Scr.* **2005**, *2005*, 1011.

(36) Ravel, B.; Newville, M. *J. Synchrotron Radiat.* **2005**, *12*, 537−541.

(37) (a) Neese, F. *ORCA 3.0.1, an Ab Inito Density Funtional and Semiempirical Program Package*; University of Bonn, Germany, 2007. (b) Neese, F. *Wiley Interdiscip. Rev.: Comput. Mol. Sci.* **2012**, *2*, 73−78.

(38) (a) Becke, A. D. *Phys. Rev. A* **1988**, *38*, 3098−3100. (b) Perdew, P. *Phys. Rev. B* **1986**, *33*, 8822−8824.

(39) (a) Schäfer, A.; Huber, C.; Ahlrichs, R. *J. Chem. Phys.* **1994**, *100*, 5829−5835. (b) Weigend, F.; Ahlrichs, R. *Phys. Chem. Chem. Phys.* **2005**, *7*, 3297−3305.

(40) Schäfer, A.; Horn, H.; Ahlrichs, R. *J. Chem. Phys.* **1992**, *97*, 2571−2577.

(41) (a) Becke, A. D. *J. Chem. Phys.* **1993**, *98*, 5648−5652. (b) Becke, A. D. *J. Chem. Phys.* **1993**, *98*, 1372−1377.